Int J Thermophys (2010) 31:2425–2439
DOI 10.1007/s10765-010-0827-4

A New Simplified Local Density Model for Adsorption of Pure Gases and Binary Mixtures

M. Hasanzadeh · M. R. Dehghani · F. Feyzi · B. Behzadi

Received: 27 June 2009 / Accepted: 14 September 2010 / Published online: 9 November 2010

Abstract Adsorption modeling is an important tool for process simulation and design. Many theoretical models have been developed to describe adsorption data for pure and multicomponent gases. The simplified local density (SLD) approach is a thermodynamic model that can be used with any equation of state and offers some predictive capability with adjustable parameters for modeling of slit-shaped pores. In previous studies, the SLD model has been utilized with the Lennard–Jones potential function for modeling of fluid–solid interactions. In this article, we have focused on application of the Sutherland potential function in an SLD–Peng–Robinson model. The advantages and disadvantages of using the new potential function for adsorption of methane, ethane, carbon dioxide, nitrogen, and three binary mixtures on two types of activated carbon are illustrated. The results have been compared with previous models. It is shown that the new SLD model can correlate adsorption data for different pressures and temperatures with minimum error.

Keywords Activated carbon · Adsorbed natural gas · Adsorption · Simplified local density · Sutherland potential function

1 Introduction

The application of natural gas (NG) as a clean and cheap energy carrier has increased in recent years when compared with other fuels. The NG share of total energy consumption is projected to increase from 23 % in 2001 to 50 % in 2020 [1]. Pipelines are a convenient and economical way for NG transport in onshore purposes, whereas

M. Hasanzadeh · M. R. Dehghani (✉) · F. Feyzi · B. Behzadi
Thermodynamics Research Laboratory, School of Chemical Engineering, Iran University of Science and Technology, Tehran, Iran
e-mail: m_dehghani@iust.ac.ir

for offshore it is challenging as the water depth and the transporting distance increase [1]. In addition, the low heat of combustion per unit volume (low relative density) is one of the most important problems in its storage, which must be solved to increase its usage. There are some solutions for transportation and NG storage. Liquefied NG (LNG), compressed NG (CNG), and adsorbed NG (ANG) can be mentioned in this regard. LNG is usually stored as a boiling liquid at a temperature about 112 K in a cryogenic tank at 0.1 MPa pressure [2]. Usually, LNG projects require large investments along with substantial NG reserves which make them economically viable just for distances longer than 5000 km [1]. CNG technology provides an effective way for shorter distance NG transportation. NG is stored as a compressed supercritical fluid at room temperature and at a maximum pressure of about 20 MPa to 25 MPa [1,2]. LNG technology needs multistage refrigeration and liquefaction to supply NG at 112 K, and CNG technology needs a multistage compression to supply NG at 20 MPa to 25 MPa. In addition, for NG storage at 112 K or 25 MPa, special instruments are needed. Adsorption of NG on porous solids is a good alternative for increasing storage capacity and improving operating conditions as well as lowering the cost of NG storage. ANG technology allows storing large amounts of NG at a relatively low pressure (3.5 MPa to 4 MPa) at room temperature in a relatively thin-walled tank filled with adsorbent. This level of pressure allows refueling the tank using a simple and cheap equipment [3].

Modeling the physical adsorption of gases onto porous materials is important in transportation and storage of NG. There are many models and theories for describing adsorption of pure gases and mixtures onto solid adsorbents. There are a wide range of theoretical approaches for modeling gas adsorption, from simple empirical fits (e.g., Freundlich isotherms [4]) to strong molecular theories based on molecular dynamics and Monte Carlo simulations. The thermodynamics of adsorption phenomena have been discussed in detail in previous studies [5–7]. There are different theories for this purpose, such as the Gibbs isotherm, the treatment of Myers and Prausnitz, vacancy solution theory, Dubinin–Polanyi theory [5], density functional theory [6], and activity-coefficient-based models [7]. The simplified local density (SLD) model is a mean-field model that superimposes the fluid–solid (fs) potential on a fluid equation of state (EOS) [8]. The SLD approach is an engineering method that can be used with any EOS and offers some predictive capability with only two temperature-independent adjustable parameters for modeling of adsorption in slit-shaped pores [9]. The SLD model so far has been applied to correlate adsorption of pure gases and mixtures onto activated carbons and coals.

The SLD model, as a modern theory for correlation of gas adsorption, has two important parts: (1) the potential function and (2) the EOS. Both parts can play an important role in the ability of the model. In all previous studies [4–10], the Lennard–Jones potential function has been utilized. In this study, we have tried to test the capabilities of another potential function. As a first step the Sutherland potential function has been selected for this purpose. So in this study, a new SLD model based on the Sutherland potential function has been presented. In order to make a good assessment of the capability of the SLD model, adsorption of different gases onto activated carbon has been modeled. Finally, the results of the modified model have been compared with previous study which had utilized the Lennard–Jones potential function.

2 SLD Model

Adsorption is expressed in several different ways. It is unambiguously defined by the Gibbs excess adsorption (Γ^{ex}), the excess number of moles per unit area of adsorbents. The excess adsorption is defined as the amount of gas contained within the system relative to the amount that would be contained if all of the void volume were occupied by gas. Two different phases are considered in the SLD model: the bulk gas and the adsorbed phase. The adsorbed phase is close to the solid surface with a very high density relative to the bulk phase [8]. Typically, the adsorbed phase density is about 10^3 to 10^4 times the bulk density, sometimes approaching the liquid-phase density.

In the first version of the SLD theory, the adsorbent was modeled as a wall, while the adsorbed gas was attached close to its surface up to a distance L [8]. However, newer studies based on the SLD model generally consider a slit geometry for the porous material [7–9]. In this case, as illustrated in Fig. 1, it could be assumed that the molecules of adsorbate reside between two-surface slit structures with a width L. The position within a slit is defined by z, where z is the orthogonal distance from the solid phase (flat surface formed by the carbon atoms inside the pore at the circumference of the wall surface). A molecule within a slit interacts with both slit surfaces. With this geometry, the excess adsorption of component i can be written as [9–11]

$$\Gamma_i^{\mathrm{ex}} = \frac{A}{2} \int_{\text{left side of slit}}^{\text{right side of slit}} \left(\rho_{\mathrm{ads},i} - \rho_{\mathrm{bulk},i}\right) \mathrm{d}z \tag{1}$$

where A is the surface area per unit mass of adsorbent, ρ the molar density, and subscripts "bulk" and "ads" refer to the bulk and adsorbed phases, respectively. The density of the adsorbed phase depends on distance, but when we take the integral over all Z, the results will be independent of Z. For a gas mixture, the subscript i indicates the property of component i in the mixture. The molar density of component i can be obtained using its mole fraction (x_i in the adsorbed phase and y_i in the bulk phase) multiplied by the total molar density. Therefore, for component i in the mixture, $\rho_{\mathrm{ads},i} \equiv x_i(z)\rho_{\mathrm{ads}}(z)$ and $\rho_{\mathrm{bulk}}\sigma_{\mathrm{ss},i} \equiv \gamma_i \rho_{\mathrm{bulk}}$.

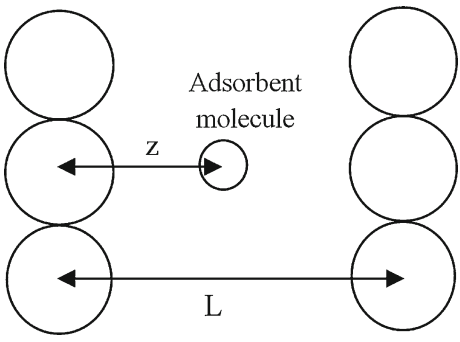

Fig. 1 Schematic of a slit-shaped pore model showing the variables used to define distances in the SLD approach [6]

For the slit geometry, the lower limit of integration is the location of the center of an adsorbed molecule touching the left plane surface ($\sigma_{ff}/2$, where σ_{ff} is the diameter of fluid molecule), and the upper limit is the location of an adsorbed molecule touching the right plane surface ($L - \sigma_{ff}/2$). At the equilibrium state, the SLD dictates that the chemical potential of the adsorbed phase at any distance from the wall is equal to that at the bulk phase, $\mu_{ads}(z) = \mu_{bulk}$. The chemical potential of the adsorbed phase is the sum of fluid–fluid (ff) and fs contributions. Since in the slit geometry a molecule of fluid interacts with two walls, the equilibrium chemical potential can be written as [10]

$$\mu(z) = \mu_{ff}(z) + \mu_{fs1}(z) + \mu_{fs2}(L - z) = \mu_{bulk} \tag{2}$$

where the subscripts "fs1" and "fs2" denote the chemical potentials arising from the first and second surfaces, respectively. In order to apply the SLD approach, it is necessary to provide the required information about ff and fs interactions. In general, the ff chemical potential can be obtained by an EOS. Simple cubic EOSs, such as Van der Waals, Peng–Robinson (PR) [12], as well as complicated EOS such as Elliott–Suresh–Donohue [13] have been used so far for this purpose [8–11]. In this study, the PR EOS has been applied due to its capability and accuracy among different cubic EOS. Previously, the 10-4 Lennard–Jones potential function was used by Lee [14] for modeling the fs interactions.

In this study, Lee's calculations have been carried out by using a Sutherland potential. The Sutherland potential consists of a hard-sphere repulsive core plus an attractive inverse power tail expressed as [15]

$$u(r) = \begin{cases} \infty & r \le \sigma \\ -\varepsilon \left(\frac{\sigma}{r}\right)^{\gamma} & r > \sigma \end{cases} \tag{3}$$

where σ is the diameter of particles, $-\varepsilon$ is the maximum potential depth, and γ is a parameter that determines the effective range of the potential. The Sutherland potential resembles the Lennard–Jones potential, for $\gamma = 6$, and therefore would be useful for studying simple fluids. This potential function is particularly useful in the treatment of multipolar interactions, and allows one to make contact with the soft core potentials such as the Lennard–Jones model [15,16]. The procedure of these calculations is given in Appendix A. Utilizing the Sutherland potential function, the fs chemical potential is derived as follows:

$$\mu_{fs}(z) = -\frac{1}{2}\pi\rho_{atoms}\varepsilon_{fs}\sum_{i=1}^{4}\frac{\sigma_{fs}^{6}}{(z' + (i-1)\,\sigma_{ss})^{4}} \tag{4}$$

Combining Eqs. 2 and 4 along with the thermodynamic relation, $\mathrm{d}\mu = kT\,\mathrm{d}\ln f$, leads to Eq. 5, which relates the bulk phase fugacity of component i, $f_{bulk,i}$, to the adsorbed phase fugacity, $f_{ads,i}$:

$$\ln\left(\frac{f_{ads,i}\,(z)}{f_{bulk,i}}\right) = -\frac{\mu_{fs,i}\,(z) + \mu_{fs,i}\,(L-z)}{kT} \tag{5}$$

The fugacity of component i in the bulk phase using the PR EOS is

$$\ln \frac{f_{\text{bulk},i}}{y_i P} = \frac{b_i}{b}(Z-1) - \ln\left(Z - \frac{Pb}{RT}\right) + \frac{a}{2\sqrt{2}RTb}\left(\frac{b_i}{b} - \frac{2\sum_j y_j a_{ij}}{a}\right) \times \ln\left(\frac{1+\rho_{\text{bulk}} b\left(1+\sqrt{2}\right)}{1+\rho_{\text{bulk}} b\left(1-\sqrt{2}\right)}\right) \tag{6}$$

where a and b are constants of the EOS, P is the pressure of the system, and $Z \equiv P/(\rho_{\text{bulk}} RT)$. The original parameters a and b are used in this study for the bulk phase [12]. The adsorbed phase fugacity can be obtained by a similar expression. It should be noted that the density, composition, and energy parameter (a) of the adsorbed phase are position-dependent (i.e., the values of these parameters vary within the slit). Therefore, the fugacity of component i in the adsorbed phase can be written by a simple extension as

$$\ln \frac{f_{\text{ads},i}(z)}{x_i(z)P} = \frac{b_i}{b}\left(\frac{P}{\rho_{\text{ads}}(z)RT} - 1\right) - \ln\left(\frac{P}{\rho_{\text{ads}}(z)RT} - \frac{Pb}{RT}\right) + \frac{a(z)}{2\sqrt{2}RTb} \times \left(\frac{b_i}{b} - \frac{2\sum_j x_j(z)a_{ij}(z)}{a(z)}\right) \ln\left(\frac{1+\rho_{\text{ads}}(z) b\left(1+\sqrt{2}\right)}{1+\rho_{\text{ads}}(z) b\left(1-\sqrt{2}\right)}\right) \tag{7}$$

where the position-dependent energy parameter of the PR EOS, $a(z)$, is taken from the work of Chen et al. [17]. The equations for $a(z)$ depend on the ratio of the slit width L to the molecular diameter σ_{ff}. These relations are given in Appendix B.

Different numbers of parameters have been used by other researchers in the SLD model. Typically, the surface area of the adsorbent (A), slit width (L), and an interaction energy parameter for each component i ($\varepsilon_{\text{fs},i}$) have been selected as adjustable parameters. However, taking the surface area of the adsorbent as an adjustable parameter is completely in contradiction with the physical nature of the adsorbent. The specific surface area of an adsorbent can be determined experimentally by characterization techniques. Reporting adsorption data on any type of adsorbent would be incomplete without determining the specific surface area. On the other hand, the slit width and interaction energy can be taken as model parameters, since they represent the essential geometry of the SLD–slit approach and the attraction force between adsorbent and gas molecules, respectively. Therefore, in this study, A is taken from the reported experimental data for each adsorbent and L, $\varepsilon_{\text{fs},i}$, σ_{ss}, and σ_{ff} are considered as adjustable parameters using both the Sutherland and Lennard–Jones potential functions.

3 Results and Discussion

The SLD–PR model has been previously applied for modeling pure gases [10,17] and mixtures [11] on activated carbon. But there seems to be insufficient information for decision making regarding the accuracy of this model, particularly for gas mixtures. In

order to examine the ability of the SLD model coupled with the PR EOS for predicting and correlating the adsorption of pure gases and mixtures, the results of the model are compared with experimental adsorption data from the literature.

3.1 Adsorption of Pure Gases

The adsorption of four pure gases including methane, ethane, carbon dioxide, and nitrogen on two types of commercially activated carbon are modeled. The required parameters for modeling pure components, including critical constants and Lennard-Jones size parameters, are listed in Table 1 [18].

The experimental data on adsorption of pure gases on two type of activated carbon (Pittsburgh BPL and Calgon F400) are extracted from Reich et al. [19] and Sudibandriyo et al. [20]. In order to estimate the adjustable parameters, the Davidon–Fletcher–Powell (DFP) algorithm has been utilized to avoid the method of direct inversion of the Hessian matrix. DFP is a well-known procedure which approximates the inverse Hessian matrix, to determine the global minimum [21]. An objective function defined by Eq. 8 was minimized.

$$OF = \frac{1}{N_{\text{exp}}} \sum_{i=1}^{N_{\text{exp}}} \left| \frac{\Gamma_{i,\text{calc}} - \Gamma_{i,\text{exp}}}{\Gamma_{i,\text{exp}}} \right| \tag{8}$$

where N_{exp} is the number of experimental data points and the subscripts "calc" and "exp" indicate the calculated and experimental values, respectively. The optimized parameters and average relative errors are listed in Table 2. It should be mentioned that the specific surface areas are taken from the experimental values ($988\ \text{m}^2 \cdot \text{g}^{-1}$ for Pittsburgh BPL [19] and $850\ \text{m}^2 \cdot \text{g}^{-1}$ for Calgon F400 [20] activated carbons), while other researchers considered it as an adjustable parameter [10,11]. Although the slit width, L, is a model parameter, it should be noted that the values of L for an adsorbent are close and on the same order of magnitude.

Here, two approaches are used for the estimation of parameters. In approach 1 as in previous studies [8–10], the molecular diameter of the solid or carbon inter-planar distance (σ_{ss}) has been considered as a constant value. In approach 2, σ_{ss} has been considered as an adjustable parameter. Both approaches have been replicated using the Lennard–Jones and the Sutherland potential functions. In the case that the Sutherland potential function is applied, as there were not any data for σ_{ff} (size parameter of the gas) in the literature, we had to determine it using mathematical minimization.

Table 1 Constants used in this study for various fluids [13]

Compound	T_c (K)	P_c (MPa)	ω	σ_{ff} (Å)
Methane	190.56	4.599	0.011	3.758
Ethane	305.32	4.872	0.099	4.443
CO_2	304.12	7.374	0.225	3.941
N_2	126.2	3.398	0.037	3.798

Table 2 Regressed pure component parameters using Lennard–Jones potential ($\sigma_{ss} = 3.35$ Å)

Component	Activated carbon	L (Å)	ε_{fs}/k (K)	AAD (%)[a]
CH_4	Pittsburgh BPL	12.02	86.21	5.38
C_2H_6	Pittsburgh BPL	13.21	111.60	7.97
CH_4	Calgon F400	11.39	99.77	1.76
CO_2	Calgon F400	12.97	118.26	7.76
N_2	Calgon F400	10.60	70.29	0.91
Average AAD (%)				4.75

[a] $\text{AAD}\ (\%) \equiv (100/N_{exp})\Sigma|(\Gamma_{calc} - \Gamma_{exp})|/\Gamma_{exp}$

Table 3 Regressed pure component parameters using Sutherland potential ($\sigma_{ss} = 3.35$ Å)

Component	Activated carbon	L (Å)	ε_{fs}/k (K)	σ_{ff}	AAD (%)[a]
CH_4	Pittsburgh BPL	19.12	76.63	8.20	5.32
C_2H_6	Pittsburgh BPL	22.15	84.23	10.12	6.63
CH_4	Calgon F400	22.96	43.59	11.39	1.02
CO_2	Calgon F400	29.30	31.60	14.29	4.75
N_2	Calgon F400	20.08	40.72	10.26	0.40
Average AAD (%)					3.62

[a] $\text{AAD}\ (\%) \equiv (100/N_{exp})\Sigma|(\Gamma_{calc} - \Gamma_{exp})|/\Gamma_{exp}$

Table 4 Regressed pure component parameters using Lennard–Jones potential (σ_{ss} as model parameter)

Component	Activated carbon	L (Å)	ε_{fs}/k (K)	σ_{ss}	AAD (%)[a]
CH_4	Pittsburgh BPL	11.41	67.04	4.14	3.76
C_2H_6	Pittsburgh BPL	12.82	64.06	5.28	6.59
CH_4	Calgon F400	11.02	50.01	5.50	1.01
CO_2	Calgon F400	12.40	60.04	5.49	7.48
N_2	Calgon F400	10.42	60.00	3.84	0.58
Average AAD (%)					3.88

[a] $\text{AAD}\ (\%) \equiv (100/N_{exp})\Sigma|(\Gamma_{calc} - \Gamma_{exp})|/\Gamma_{exp}$

In approach 1, σ_{ss} is fixed at 3.35 Å based on a graphite crystalline structure [10–12]. The other adjusted parameters and average relative errors for both potential functions are listed in Tables 2 and 3.

In approach 2, σ_{ss} along with L and ε_{fs} are considered as adjustable parameters. The regressed parameters are listed in Tables 4 and 5.

As shown in Tables 2–5, in all cases, the use of Sutherland potential functions caused a decrease in the absolute average deviation, regardless of the number of adjusted parameters. However, the number of adjusted parameters is effective in better fitting, but considering Tables 3 and 4, it will be clear that the Sutherland potential shows better results using an equal number of adjusted parameters. It is worth mentioning that

Table 5 Regressed pure component parameters using Sutherland potential (σ_{ss} as model parameter)

Component	Activated carbon	L (Å)	ε_{fs}/k (K)	σ_{ff}	σ_{ss}	AAD (%)[a]
CH_4	Pittsburgh BPL	20.00	72.02	8.76	2.79	4.99
C_2H_6	Pittsburgh BPL	17.11	104.90	7.00	6.06	6.48
CH_4	Calgon F400	19.21	43.60	9.00	6.77	1.01
CO_2	Calgon F400	35.00	17.47	17.34	0.93	4.07
N_2	Calgon F400	7.95	87.23	2.40	8.22	0.35
Average AAD (%)						3.38

[a] AAD (%) $\equiv (100/N_{exp})\Sigma|(\Gamma_{calc} - \Gamma_{exp})|/\Gamma_{exp}$

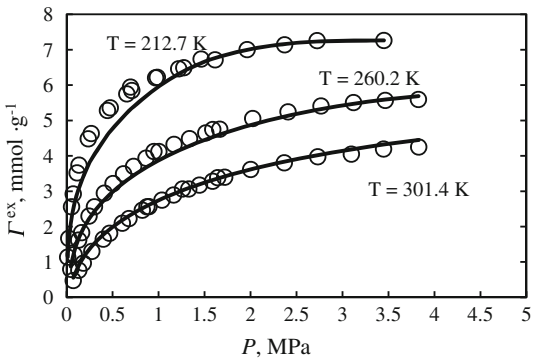

Fig. 2 Methane adsorption isotherms on Pittsburgh BPL activated carbon. Symbols are experimental data [18], and lines are the results from SLD–PR model

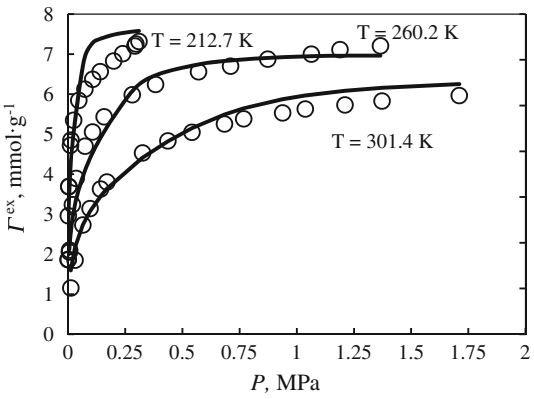

Fig. 3 Ethane adsorption isotherms on Pittsburgh BPL activated carbon. Symbols are experimental data [18], and lines are the results from SLD–PR model

the modified SLD model can correlate the adsorption of CO_2 better than the original one. Previously, Gill-Villegas et al. [16] applied different potential functions in the SAFT EOS and found that the Sutherland potential gives better results in modeling polar components like CO_2.

In Figs. 2–5, the correlated adsorption isotherms for Pittsburgh BPL activated carbon are depicted.

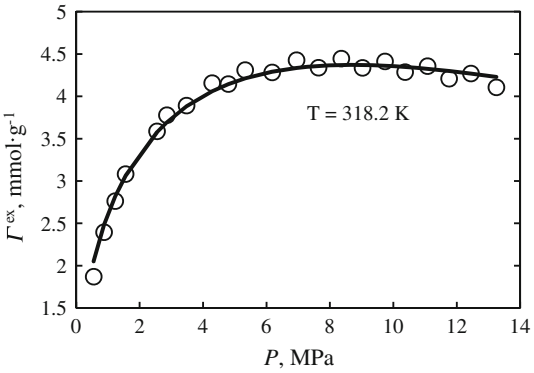

Fig. 4 Methane adsorption isotherm on Calgon F400 activated carbon. Symbols are experimental data [18], and line represents the results from SLD–PR model

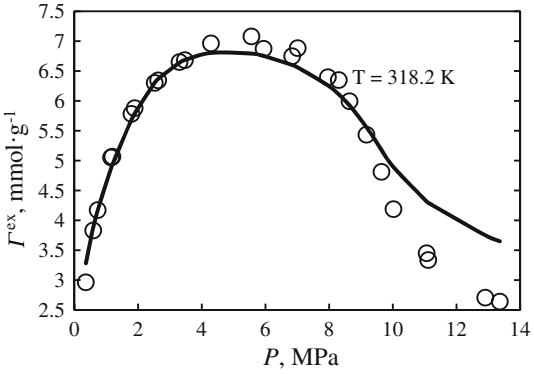

Fig. 5 CO_2 adsorption isotherm on Calgon F400 activated carbon. Symbols are experimental data [18], and line represents the results from SLD–PR model

In general, it can be concluded that there is a good agreement between the experimental data and the correlated results of the SLD–PR model, except in the case of CO_2 and ethane at high pressures. Our preliminary tests on different cubic EOS like PR showed that they would all give similar results as PR. Therefore, this behavior may be raised from the application of any of the general forms of the cubic EOS. Probably, the SAFT EOS families give better results for associative compounds.

3.2 Adsorption Modeling for Binary Mixtures

The lack of useful experimental data for binary mixtures is a serious problem in adsorption modeling of multicomponent gases. This fact arises from the experimental difficulties encountered in measurement of adsorption of gas mixtures. Three binary mixtures, including $CH_4 + N_2$, $CH_4 + CO_2$, and $N_2 + CO_2$, are considered in this section. The data were taken from Ref. [19]. The carbon inter-planar distance, σ_{ss}, has been fixed at 3.35 Å. The slit width L and energy parameter (ε_{fs}) have been adjusted using mathematical minimization. The optimized parameters and the absolute average deviation when using the Lennard–Jones and Sutherland potential functions have been listed in Tables 6 and 7.

Table 6 Regressed parameters for multicomponent gas adsorption using Lennard–Jones potential

System	L (Å)	ε_{fs}/k (K)		AAD (%)[a]
		(1)	(2)	
Methane (1) + N_2 (2)	10.45	85.37	58.83	12.76
Methane (1) + CO_2 (2)	10.02	64.18	67.30	18.57
N_2 (1) + CO_2 (2)	9.27	45.98	69.80	8.36
Average AAD (%)				13.23

[a] $\text{AAD}\ (\%) \equiv (100/N_{exp})\Sigma|(\Gamma_{calc} - \Gamma_{exp})|/\Gamma_{exp}$

Table 7 Regressed parameters for multicomponent gas adsorption using Sutherland potential

System	L (Å)	ε_{fs}/k (K)		σ_{ff} (Å)		AAD (%)[a]
		(1)	(2)	(1)	(2)	
Methane (1) + N_2 (2)	25.33	44.37	123.70	8.42	5.59	10.54
Methane (1) + CO_2 (2)	13.16	113.66	116.40	4.25	4.07	11.83
N_2 (1) + CO_2 (2)	8.14	88.71	77.99	4.34	4.93	6.32
Average AAD (%)						9.56

[a] $\text{AAD}\ (\%) \equiv (100/N_{exp})\Sigma|(\Gamma_{calc} - \Gamma_{exp})|/\Gamma_{exp}$

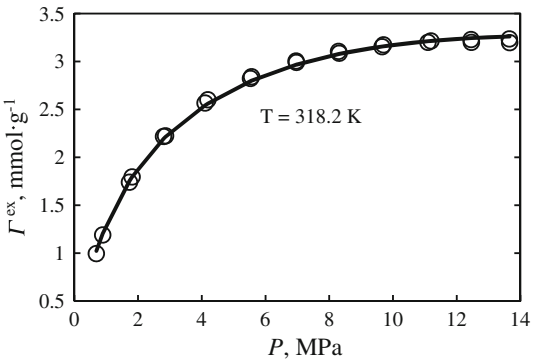

Fig. 6 N_2 adsorption isotherm on Calgon F400 activated carbon. Symbols are experimental data [19], and line represents the results from SLD–PR model

In Figs. 6–12, the results for the binary systems are shown. As for pure gases, the results for CO_2 and ethane adsorption are not in good agreement with the experimental data in comparison with experimental uncertainty.

4 Conclusion

The SLD–PR model was applied to correlate adsorption of pure gases and binary mixtures on activated carbon. In this study, the Sutherland and Lennard–Jones intermolecular potential functions were used to predict gas adsorption on the solid phase by the SLD model. The capability of the presented model for pure gases indicates that it is

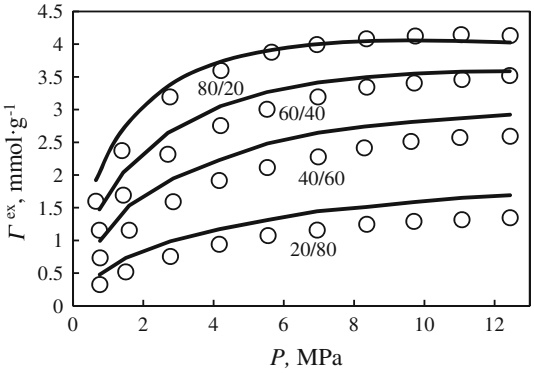

Fig. 7 Methane adsorption isotherms at 318.2 K on Calgon F400 activated carbon, in the mixture methane + N_2. Symbols are experimental data [19], and lines are the results from SLD–PR model. Legends on curves indicate the methane/N_2 ratio in the feed gas

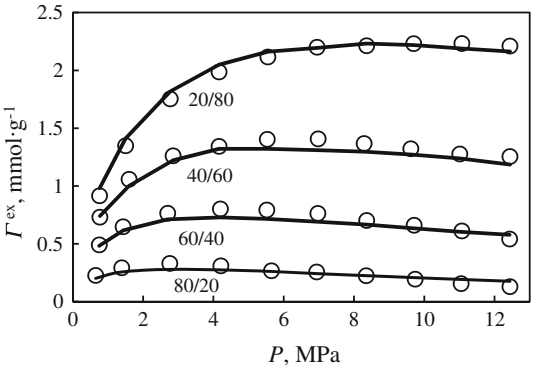

Fig. 8 N_2 adsorption isotherms at 318.2 K on Calgon F400 activated carbon, in the mixture methane + N_2. Symbols are experimental data [19], and lines are the results from SLD–PR model. Legends on curves indicate the methane/N_2 ratio in the feed gas

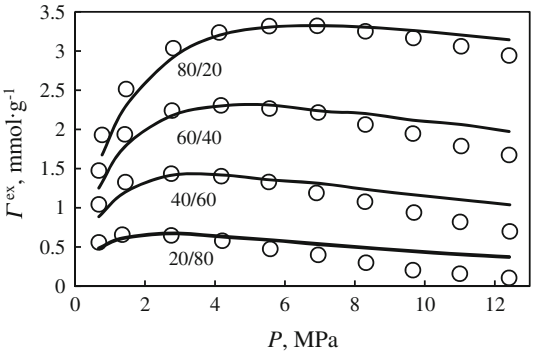

Fig. 9 Methane adsorption isotherms at 318.2 K on Calgon F400 activated carbon, in the mixture methane + CO_2. Symbols are experimental data [19], and lines are the results from SLD–PR model. Legends on curves indicate the methane/CO_2 ratio in the feed gas

consistent with the physics of adsorption. The model parameters were regressed using two approaches for pure gases: considering as a constant or as a model parameter. Meanwhile, only the physically meaningful parameters were considered as adjustable parameters. Simple intermolecular potentials, such as those considered in this study, are an idealized view of interactions between atoms. These potentials assume spherical

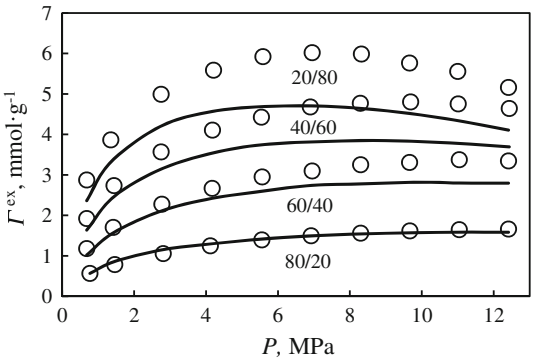

Fig. 10 CO_2 adsorption isotherms at 318.2 K on Calgon F400 activated carbon, in the mixture methane + CO_2. Symbols are experimental data [19], and lines are the results from SLD–PR model. Legends on curves indicate the methane/CO_2 ratio in the feed gas

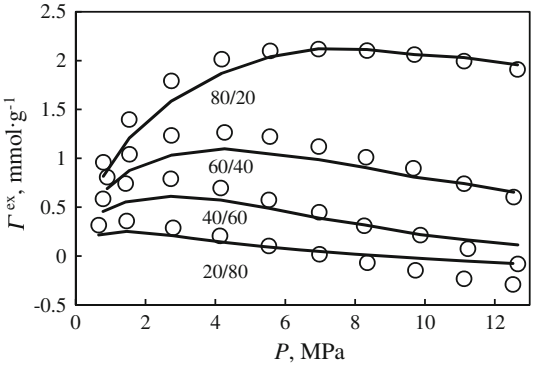

Fig. 11 N_2 adsorption isotherms at 318.2 K on Calgon F400 activated carbon, in the mixture $N_2 + CO_2$. Symbols are experimental data [19], and lines are the results from SLD–PR model. Legends on curves indicate the N_2/CO_2 ratio in the feed gas

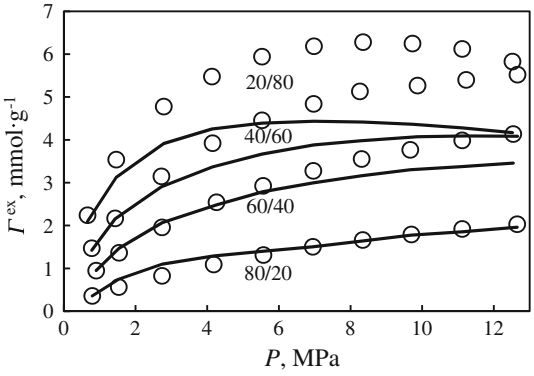

Fig. 12 CO_2 adsorption isotherms at 318.2 K on Calgon F400 activated carbon, in the mixture $N_2 + CO_2$. Symbols are experimental data [19], and lines are the results from SLD–PR model. Legends on curves indicate the N_2/CO_2 ratio in the feed gas

molecules without polar effects. For non-spherical and polar molecules (e.g., C_2H_6 and CO_2), more complicated potentials considering molecular shape and polarity should yield more accurate results. The Sutherland potential function shows a lower average deviation, in both approaches of taking σ_{ss} as a constant or a model parameter, in comparison with Lennard–Jones, especially for CO_2 because of its polar nature. It is

shown that the new SLD model can correlate adsorption data for different pressures and temperatures with minimum error.

On the other hand, the extension of the model to multicomponent adsorption led to large deviations from experimental data. It means that much work must be done to improve the SLD model for prediction of gas mixtures.

Appendix A: Calculational Procedure of Lee Using the Sutherland Potential

If the coordinates x and y have been selected to lie on the interfacial plane such that the solid occupies the region $Z < 0$, a gas molecule at a vertical distance $Z > 0$ above the surface will interact with all the atoms of the solid (on the surface as well as below). For fixed $x - y$ coordinates, the forces on a gas molecule at any $Z < 0$ due to the wall represent the sum of pair interactions between the gas molecule and all solid atoms:

$$w(z)\Big|_{x,y} = \sum_{\text{atom } i} w^{\text{LJ}}(r_i)\Big|_{x,y} \tag{A1}$$

where the subscripts x and y denote the fixed values x and y for the gas molecule, and r_i is the distance between the solid atom i below and the gas molecule above.

If in the limit of small solid atoms, the surface appears *smooth* to the gas molecules, the sum over the layers of atoms can be replaced by an integral. Lee's integral for the Sutherland potential can be written as

$$w(z) = \sum_{k \text{ layers}} \int_{-\infty}^{+\infty} \mathrm{d}x \int_{-\infty}^{+\infty} \mathrm{d}y 4\varepsilon_{\text{gs}} \left(\frac{\sigma_{\text{gs}}^6}{\left(x^2 + y^2 + z^2\right)^3} \right) \tag{A2}$$

The result of this integral is

$$w = -\frac{1}{2}\pi \varepsilon_{\text{gs}} \sum_{k \text{ layers}} \frac{\sigma_{\text{gs}}^6}{\sigma_{\text{ss}}^4} \left(\frac{1}{z^* + k} \right)^4 \tag{A3}$$

where ε_{gs} is the gas–solid energy parameter, σ_{gs} is the gas–solid size parameter, σ_{ss} is the Sutherland size parameter for the solid–solid atom interaction, and $z = z/\sigma_{\text{ss}}$ is the reduced vertical distance of the gas molecule above the surface.

Appendix B: Expressions for the Position-Dependent Energy Parameter [16]

For $L/\sigma_{ff} \geq 3$, $a(z)$ is given by

$$\frac{a(z)}{a_{bulk}} = \begin{cases} \frac{3}{8}\left[\frac{z}{\sigma_{ff}} + \frac{5}{6} - 1\Big/3\left(\frac{L-z}{\sigma_{ff}} - 0.5\right)^3\right] & \text{for } 0.5 \leq \frac{z}{\sigma_{ff}} \leq 1.5 \\ \frac{3}{8}\left[\frac{8}{3} - 1\Big/3\left(\frac{z}{\sigma_{ff}} - 0.5\right)^3 - 1\Big/3\left(\frac{L-z}{\sigma_{ff}} - 0.5\right)^3\right] & \text{for } 1.5 \leq \frac{z}{\sigma_{ff}} \leq \frac{L}{\sigma_{ff}} - 1.5 \\ \frac{3}{8}\left[\frac{L-z}{\sigma_{ff}} + \frac{5}{6} - 1\Big/3\left(\frac{z}{\sigma_{ff}} - 0.5\right)^3\right] & \text{for } \frac{L}{\sigma_{ff}} - 1.5 \leq \frac{z}{\sigma_{ff}} \leq \frac{L}{\sigma_{ff}} - 0.5 \end{cases} \quad \text{(B1)}$$

For $2 \leq L/\sigma_{ff} \leq 3$,

$$\frac{a(z)}{a_{bulk}} = \begin{cases} \frac{3}{8}\left[\frac{z}{\sigma_{ff}} + \frac{5}{6} - 1\Big/3\left(\frac{L-z}{\sigma_{ff}} - 0.5\right)^3\right] & \text{for } 0.5 \leq \frac{z}{\sigma_{ff}} \leq \frac{L}{\sigma_{ff}} - 1.5 \\ \frac{3}{8}\left(\frac{L}{\sigma_{ff}} - 1\right) & \text{for } \frac{L}{\sigma_{ff}} - 1.5 \leq \frac{z}{\sigma_{ff}} \leq 1.5 \\ \frac{3}{8}\left[\frac{L-z}{\sigma_{ff}} + \frac{5}{6} - 1\Big/3\left(\frac{z}{\sigma_{ff}} - 0.5\right)^3\right] & \text{for } 1.5 \leq \frac{z}{\sigma_{ff}} \leq \frac{L}{\sigma_{ff}} - 0.5 \end{cases} \quad \text{(B2)}$$

For $1.5 \leq L/\sigma_{ff} \leq 2$,

$$\frac{a(z)}{a_{bulk}} = \frac{3}{8}\left(\frac{L}{\sigma_{ff}} - 1\right) \quad \text{(B3)}$$

For a small slit where $1 \leq L/\sigma_{ff} \leq 1.5$, the value of Eq. A3 in Appendix A at $L/\sigma_{ff} = 1.5$ must be used, i.e., $a(z)/a_{bulk} = 3/16$.

References

1. M. Economides, R. Oligney, A. Demarchos, SPE. 62884 (2000)
2. D. Lozano-Castello, J. Alcaniz-Monge, M.A. de la Casa-Lillo, D. Cazorla-Amoros, A. Linares-Solano, Fuel **81**, 1777 (2002)
3. Y. Ginzburg, in *23rd World Gas Conference*, Amsterdam, 2006
4. F. Rouquerol, J. Rouquerol, K. Sing, *Adsorption by Powders and Porous Solids* (Academic Press, San Diego, CA, 1999)
5. D.M. Ruthven, *Principles of Adsorption and Adsorption Processes* (Wiley, New York, 1984)
6. H. Pan, J.A. Ritter, P.B. Balbuena, Ind. Eng. Chem. Res. **37**, 1159 (1998)
7. M.R. Riazi, A.R. Khan, J. Colloid Interface Sci. **210**, 309 (1999)
8. B. Rangarajan, C.T. Lira, R. Subramanian, AIChE J. **41**, 838 (1995)
9. A.D. Soule, C.A. Smith, X. Yang, C.T. Lira, Langmuir **17**, 2950 (2001)
10. J.E. Fitzgerald, M. Sudibandriyo, Z. Pan, R.L. Robinson, K.A.M. Gasem, Carbon **41**, 2203 (2003)
11. J.E. Fitzgerald, R.L. Robinson, K.A.M. Gasem, Langmuir **22**, 9610 (2006)
12. D.Y. Peng, D.B. Robinson, Ind. Eng. Chem. Fund. **15**, 59 (1976)
13. J.R. Elliott, S.J. Suresh, M.D. Donohue, Ind. Eng. Chem. Res. **29**, 1476 (1990)
14. L.L. Lee, *Molecular Thermodynamics of Nonideal Fluids* (Butterworths, Stoneham, MA, 1988)
15. A. Diez, J. Largo, J.R. Solana, Fluid Phase Equilib. **253**, 67 (2007)
16. A. Gill-Villegas, A. Galindo, P.J. Whitehead, S.J. Mills, G. Jackson, A.N. Burgess, J. Chem. Phys. **106**, 4168 (1997)
17. J.H. Chen, D.S.H. Wong, C.S. Tan, R. Subramanian, C.T Lira, M. Orth, Ind. Eng. Chem. Res. **36**, 2808 (1997)

18. B.E. Poling, J.M. Prausnitz, J.P. O'Connell, *The Properties of Gases and Liquids* (McGraw-Hill, New York, 2001)
19. R. Reich, W.T. Ziegler, K.A. Rogers, Ind. Eng. Chem. Process Des. Dev. **19**, 336 (1980)
20. M. Sudibandriyo, Z. Pan, J.E. Fitzgerald, R.L. Robinson, K.A.M. Gasem, Langmuir **19**, 5323 (2003)
21. M.R. Dehghani, H. Modarress, J. Mol. Liq. **142**, 45 (2008)